

# Integrated Machine Learning and Survival Analysis Modeling for Enhanced Chronic Kidney Disease Risk Stratification

Zachary Dana  
Ahmed Ammar Naseer  
Botros Toro  
Sumanth Swaminathan

*Vironix Health Inc, Austin, TX, USA*

ZDANA@VIRONIX.AI  
AANASEER22@GMAIL.COM  
BTORO@VIRONIX.AI  
SSWAMI@VIRONIX.AI

## Abstract

Chronic kidney disease (CKD) is a significant public health challenge, often progressing to end-stage renal disease (ESRD) if not detected and managed early. Early intervention, warranted by silent disease progression, can significantly reduce associated morbidity, mortality, and financial burden. In this study, we propose a novel approach to modeling CKD progression using a combination of machine learning techniques and classical statistical models. Building on the work of Liu et al. (2023), we evaluate linear models, tree-based methods, and deep learning models to extract novel predictors for CKD progression, with feature importance assessed using Shapley values. These newly identified predictors, integrated with established clinical features from the Kidney Failure Risk Equation, are then applied within the framework of Cox proportional hazards models to predict CKD progression.

**Keywords:** Chronic kidney disease; Cox proportional hazards; feature selection; machine learning

**Data and Code Availability** Code utilized in this study is available as supplemental material. We make use of the publicly available MIMIC-IV (Medical Information Mart for Intensive Care, Version IV) clinical database (Johnson et al., 2024) in our experiments. MIMIC-IV consists of 364,627 thousand medical records for patients admitted in critical care units of the Beth Israel Deaconess Medical Center in Boston, MA from 2008 to 2022. It is an update of the earlier MIMIC-III database (Johnson et al., 2024).

**Institutional Review Board (IRB)** This paper uses the publicly available and de-identified MIMIC-IV dataset, which does not require IRB approval.

## 1. Introduction

Chronic kidney disease (CKD) is a major public health concern, characterized by silent disease progression that can lead to end-stage renal disease (ESRD) and the need for kidney transplantation if not detected early (Bai et al., 2022). CKD affects millions globally and is associated with significant morbidity, mortality, and healthcare costs (Kerr et al., 2012). The gradual decline in kidney function in CKD patients often goes unnoticed until the disease has advanced to a critical stage (Kalantar-Zadeh et al., 2021). Early intervention in CKD can improve the quality of life and reduce healthcare expenses by slowing disease progression (Kalantar-Zadeh et al., 2021).

Predictive models and dynamic risk stratification algorithms can enable identification of patients at high risk of CKD degeneration. These models facilitate timely modifications in patient management, including adjustments to medication, diet, sleep, and exercise regimens, thereby improving patient outcomes (Xiao et al., 2019). In recent years, machine learning (ML) techniques have shown great promise in healthcare applications, providing powerful tools for predictive modeling and risk stratification (Appendix B).

In this study, we evaluate an approach to modelling the progression of CKD stages using a combination of ML techniques and classical statistical models. By extending the work proposed by Liu et al. (2023) we evaluate the use of linear models, tree-based models, and deep learning models in extracting novel predictors for CKD degeneration, determined by Shapley values. These novel predictors are then used in conjunction with clinically established kidney failure risk equation (KFRE) features (Appendix C) to model

the progression of CKD using cox proportional hazards models (CPHMs).

**Contributions.** **1.** Identification of potential novel predictors for CKD progression: By leveraging machine learning models, Shapley value analysis, and classical survival models, this work identifies new features beyond the established clinical predictors in the KFRE-8 model to aid in predicting CKD progression. **2.** Improved predictive performance for CKD progression: The integration of machine learning-derived predictors with classical Cox proportional hazards models leads to improved predictive accuracy, as demonstrated by higher C-index and lower Brier scores. **3.** Extension of Liu et al. (2023) methodology: by exploring additional models for feature selection and extending the Cox proportional hazards modeling to CKD progression.

## 2. Method

### 2.1. Pipeline

Our approach follows a structured pipeline for feature selection and modeling. Let  $\mathcal{D} = \{\mathbf{x}_i\}_{i=1}^M$ , denote a dataset where each  $\mathbf{x}_i \in \mathbb{R}^N$  represents a feature vector. Let  $f : \mathbb{R}^N \mapsto \{0, 1\}$  represent a binary classifier (Appendix D). We first train the classifier  $f(\cdot; \theta) : \mathbb{R}^n \mapsto \{0, 1\}$  on  $\mathcal{D}^{Tr} \in \mathbb{R}^{P \times n}$  a training data subset from  $\mathcal{D}$ . After training, we compute the Shapley  $\phi_i$  for each feature  $x_i$  (Appendix E). The top  $j$  features with the highest mean Shapley values are selected, forming the set  $F_s$ . Next, we combine  $F_s$  with the KFRE-8 feature set  $F_{\text{KFRE-8}}$  by taking their union, defined as  $F = F_s \cup F_{\text{KFRE-8}}$ . The dataset  $\mathcal{D}$  is then reduced to include only features in  $F$ . Finally, a CPHM is trained on this reduced data set to predict CKD progression (Appendix F), evaluating the novel predictors’ efficacy within the framework of survival analysis. Figure 1 illustrates the modelling pipeline used here. This paper expands the methodology proposed by Liu et al. (2023) through the incorporation of a diverse range of model architectures in the feature selection stage, and extends the application to CKD.

## 3. Experiments

### 3.1. Data and data handling

**MIMIC-IV.** We extracted the complete subset of patients from MIMIC-IV with documented CKD di-

agnoses, as indicated by seven relevant ICD-9 codes described in Table 1, yielding a cohort of 14,012 patients. Using this subset, we define a binary variable to indicate CKD progression, deemed observed if a patient is diagnosed with a more advanced CKD stage at any time after an earlier diagnosis of a less severe stage. Among the patients in the cohort, 1,483 (10.6%) experienced CKD stage progression over a median follow-up period of 111.5 days (IQR 6.0-910.25). The feature selection models, were trained on a high-dimensional input set, including a combined 1373 demographic, diagnostic, and lab recording features; the full characteristics of the former are summarized in Table 2.

### 3.2. Feature selection

#### 3.2.1. MODELS

We evaluate the performance of five binary classifiers for the feature selection component of the pipeline: logistic regression (LR), decision tree (DT), random forest (RF), extreme gradient boosting (XGBoost), fully connected neural networks (FCNNs), and residual neural network (ResNet). The linear models (Appendix D.1) and tree-based methods (Appendix D.2) were trained with the logarithmic loss function as the objective criterion, and hyperparameters were selected through Bayesian optimization; detailed search spaces and optimized values for the latter are provided in Table 4. For logistic regression, the solver was specified a `lbfgs`, and maximum iterations set to 1000.

The neural networks (Appendix D.3) utilize binary cross-entropy loss with logits and the Adam optimizer. The FCNN model was configured with 4 hidden layers containing 512, 256, 128, and 1 neuron, each followed by a dropout layer with the rate set to 0.2. For ResNet, we used 3 residual blocks, each consisting of 2 fully-connected layers with a hidden dimension of 64. Single fully-connected layers were applied prior to and following the residual blocks, yielding an architecture with 8 layers in total. Rectified linear unit (ReLU) activation was applied in both architectures. The learning rate, weight decay (L2 regularization), maximum epoch, and early stopping hyperparameters are reported in Table 3.

All models were trained and evaluated across five distinct data splits, utilizing unique random seeds for cross-validation. For the linear and tree-based methods, the training sets were further divided into five validation folds to support Bayesian optimization,

prior to applying the tuned hyperparameter values in model cross-validation with the complete data splits.

### 3.2.2. FEATURES

For each binary classifier, we identified the 40 features with the highest mean absolute Shapley values. The union of these top features, along with those defined in KFRE-8, was then selected as the final feature set. Because of the computational infeasibility of calculating Shapley values as defined in equation (9) for the large number of features, we utilized shapley additive explanations (SHAP) (Lundberg and Lee, 2017) to approximate these values. Specifically, SHAP values were computed using the TreeExplainer (Lundberg et al., 2020) for tree-based models, the LinearExplainer for linear models, and the DeepExplainer for deep learning models.

### 3.3. Cox proportional hazards model

Following the feature selection, CPHMs were fitted to explore the associations between the identified novel predictors and CKD stage progression. The data for the final feature set obtained from each binary classifier were used to train the CPHMs. Additionally, a baseline CPHM was trained using only the KFRE-8 features to serve as a control. The CPHMs were implemented with a penalizer set to 0.0007, the minimum value necessary to prevent overfitting. Model fitting involved five-fold cross-validation, and the optimal model was selected based on the highest average concordance Index (C-index) (Appendix G.2) across the validation sets. The models with the best performance, as indicated by the highest average C-index, were preserved for further analysis, along with the corresponding training and testing datasets. The proportional hazards assumption was evaluated using Schoenfeld residuals. Additionally, Brier score (Appendix G.3) and dynamic area under receiving operating characteristic curve (AUROC) plots (Appendix G.1) were generated for the full set of hazards models, offering an assessment of the alignment between predicted risks and observed outcomes over time.

We computed Brier score at 5-year for assessing overall model performance and C-index for assessing risk discrimination. We used the two sets of baseline hazard at 5-year and model coefficients (i.e. “beta values”) yielded from these two Cox models to compute the 5-year risks and prognostic index (i.e. variable beta) of each participant in the training (80%) and test (20%) data, respectively. These 5-year risks

were subsequently used to compute Brier score at 5 years and prognostic indices were used to compute C-index using the training and test data, respectively.

## 4. Results and Discussion

### 4.1. Feature selection results

**AUROC.** Table 5 shows the AUROC scores obtained by the ML models used in the feature extraction process. The comparison of models based on AUROC shows that XGBoost performs the best, with the highest average AUROC of 0.7796 and a best score of 0.8105. DT follows with an average score of 0.7283, and the best-performing model scores 0.7799. LR achieves an average AUROC of 0.7027, performing slightly below DT. RF performs the worst, with an average of 0.5796. Deep learning models such as FCNN and ResNet perform similarly, with average AUROC values of 0.6612 and 0.6540, respectively.

**SHAP.** Figures 2, 3, 4, 5, 6, and 7 show the top 40 mean absolute SHAP values obtained by the feature selection models. Across nearly all models, features related to creatinine (e.g., creatinine mean, max, last, and median) consistently rank among the most important predictors. This trend is particularly observed in the XGBoost, RF, LR, and DT models. Renal dialysis status appears as one of the top contributors in almost all models, particularly in ResNet, LR, FCNN, and DT. Urea nitrogen frequently appears in the top set of important features, particularly in the XGBoost, RF, and ResNet models. For deep learning models, ResNet and FCNN, features such as “Coronary atherosclerosis of native coronary artery” and “Coronary artery disease” appear as highly important. Markers such as mean corpuscular hemoglobin concentration (MCHC), mean corpuscular hemoglobin (MCH), neutrophils, platelet count, and eosinophils feature prominently across models. Potassium-related features show importance in several models, particularly in XGBoost, ResNet, and RF. In models such as ResNet and FCNN, we see several features related to more specific conditions, like unspecified essential hypertension and other hyperlipidemia. Features related to chronic conditions, like unspecified essential hypertension, acute kidney failure, and diabetes with renal manifestations, are consistently seen in models like LR, ResNet, and FCNN.

## 4.2. Cox proportional hazards model results

**C-index.** Table 6 provides the results for C-index obtained using the CPHMs. The LR-augmented Cox model performs the best, with an average of 0.8900 and a best score of 0.9016. Other models, including XGBoost-Augmented Cox and ResNet-Augmented Cox, show competitive results, both achieving an average of around 0.8876 and 0.8878, respectively. The baseline Cox model, with an average C-index of 0.8820, is outperformed by all the augmented models. DT-Augmented Cox and RF-Augmented Cox models show slightly lower averages at 0.8855 and 0.8865, respectively.

**Brier score.** The CPHM Brier score results are plotted at 5 years in Appendix J, and reported at annual intervals in Table 7. The XGBoost-augmented Cox model outperforms the other models across most time intervals, particularly at 1 year (0.0289), 4 years (0.0750), and 5 years (0.0801). FCNN-Augmented Cox achieves the best Brier scores at 2 years (0.0485) and 3 years (0.0625). DT-Augmented Cox also shows competitive performance, especially at 2 years with a score of 0.0496. Baseline Cox shows higher Brier scores across the intervals, especially at 5 years (0.1120), indicating less accurate predictions compared to the augmented models.

**Dynamic AUROC.** The CPHM dynamic AUROC results are plotted at 5 years in Appendix K, and reported at annual intervals in Table 8. The LR-Augmented Cox model performs best for the first 3 years, with the highest AUROC of 0.9634 at 1 year, 0.9499 at 2 years, and 0.9453 at 3 years. However, at the 4- and 5-year intervals, XGBoost-Augmented Cox achieves the highest AUROC of 0.9376 and 0.9507, respectively. Baseline Cox performs consistently, but its scores decline slightly over time, especially at 5 years (0.9113). Other augmented models, such as FCNN and ResNet, show stable but slightly lower AUC scores compared to the best-performing models.

## 4.3. Discussion

Across all models, SHAP analysis reveals that traditional kidney function markers, particularly creatinine (e.g., mean, max, last, and median values) and renal dialysis status, are consistently the most important features, affirming their clinical relevance in CKD progression. Additionally, urea nitrogen (max and mean) is another key renal marker that ranks

highly, emphasizing its significance in predicting disease outcomes. These results indicate that the models correctly prioritize well-established CKD markers, providing confidence in the feature selection process.

SHAP analysis also highlights several non-traditional features that are not part of the KFRE-8 model but rank highly across models. Markers such as MCHC, MCH, neutrophils, and platelet count — blood-related features not typically associated with CKD — emerge as important predictors. Their relevance suggests that systemic factors related to hematologic and immune responses may play a role in CKD progression. Though it is worth noting that this could also be a result of the patient population used in this study. Furthermore, potassium levels appear highly in models such as XGBoost and ResNet, reflecting the importance of this for CKD progression prediction. Additionally, deep learning models such as ResNet and FCNN bring attention to cardiac-related conditions, including coronary atherosclerosis and coronary artery disease, which are identified as significant predictors. This suggests that cardiovascular conditions, often comorbid with CKD, should be considered as potential predictors in models for CKD progression. These findings underscore the value of machine learning in surfacing predictors that may extend beyond traditional renal markers, contributing to a more comprehensive understanding of CKD.

The application of SHAP values enables not only the identification of important features but also their interpretability, allowing for the validation of established predictors while suggesting new avenues for research. By identifying features not present in the KFRE-8 model, such as creatinine levels, urea nitrogen, potassium, and blood-related markers, this analysis highlights the potential for integrating additional predictors into CKD progression models. This could improve the predictive accuracy and provide deeper insights into disease mechanisms.

## 5. Limitations

The identification of novel predictors requires further validation, as these features may serve as proxies for unmodeled processes. Moreover, the reliance on the MIMIC-IV dataset, which is derived from an emergency room setting, limits the generalizability of our findings to patient cohorts within this environment. To strengthen the robustness of our results, validation using an external cohort is necessary to confirm the findings and improve the accuracy of the method.

## 6. Conclusion

In this study, we propose and validate a novel approach for predicting CKD progression by integrating machine learning models with classical statistical techniques. This method identifies potential novel predictors of CKD progression while confirming established risk factors. Our results show that combining machine learning-based feature selection with Cox proportional hazards models enhances predictive performance for CKD.

## References

- Qiong Bai, Chunyan Su, Wen Tang, and Yike Li. Machine learning to predict end stage kidney disease in chronic kidney disease. *Scientific Reports*, 12(1): 8377, 2022. doi: 10.1038/s41598-022-12316-z.
- Leo Breiman. Random forests. *Machine learning*, 45(1):5–32, 2001.
- Leo Breiman, Jerome Friedman, Charles J Stone, and Richard A Olshen. *Classification and regression trees*. Wadsworth International Group, 1984.
- Glenn W Brier. Verification of forecasts expressed in terms of probability. *Monthly weather review*, 78(1):1–3, 1950.
- Tianqi Chen and Carlos Guestrin. Xgboost: A scalable tree boosting system. In *Proceedings of the 22nd ACM SIGKDD International Conference on Knowledge Discovery and Data Mining*, KDD '16, pages 785–794, New York, NY, USA, 2016. Association for Computing Machinery. ISBN 9781450342322. doi: 10.1145/2939672.2939785. URL <https://doi.org/10.1145/2939672.2939785>.
- D. R. Cox. Regression models and life-tables. *Journal of the Royal Statistical Society: Series B (Methodological)*, 34(2):187–220, 1972. ISSN 0035-9246. doi: 10.1111/j.2517-6161.1972.tb00899.x. URL <https://doi.org/10.1111/j.2517-6161.1972.tb00899.x>.
- National Kidney Foundation. Kidney failure and the kidney failure risk equations (kfre): What you need to know. <https://www.kidney.org/content/kidney-failure-and-kidney-failure-risk-equations>. June 2023. Accessed: 2024-01-08.
- Frank E Harrell, Robert M Califf, David B Pryor, Kerry L Lee, and Robert A Rosati. Evaluating the yield of medical tests. *Jama*, 247(18):2543–2546, 1982.
- Kaiming He, Xiangyu Zhang, Shaoqing Ren, and Jian Sun. Deep residual learning for image recognition. In *Proceedings of the IEEE Conference on Computer Vision and Pattern Recognition (CVPR)*, pages 770–778, June 2016. doi: 10.1109/CVPR.2016.90.
- David W. Hosmer, Stanley Lemeshow, and Rodney X. Sturdivant. *Applied Logistic Regression*. John Wiley & Sons, Hoboken, New Jersey, 3rd edition, 2013. ISBN 978-0470582473. doi: 10.1002/9781118548387.
- Alistair E. W. Johnson, Tom J. Pollard, Lu Shen, and Li wei H. Lehman. MIMIC-IV documentation, 2024. URL <https://mimic.mit.edu/docs/iv/>. Accessed: 2024-08-08.
- Kamyar Kalantar-Zadeh, Tazeen H Jafar, Dorothea Nitsch, Brendon L Neuen, and Vlado Perkovic. Chronic kidney disease. *The Lancet*, 398(10302): 786–802, 2021.
- Marion Kerr, Benjamin Bray, James Medcalf, Donal J O’Donoghue, and Beverley Matthews. Estimating the financial cost of chronic kidney disease to the NHS in England. *Nephrology Dialysis Transplantation*, 27(suppl.3):iii73–iii80, 2012.
- Yann LeCun, Yoshua Bengio, and Geoffrey Hinton. Deep learning. *Nature*, 521(7553):436–444, May 2015. doi: 10.1038/nature14539.
- Xiaonan Liu, Davide Morelli, Thomas J Littlejohns, David A Clifton, and Lei Clifton. Combining machine learning with Cox models to identify predictors for incident post-menopausal breast cancer in the UK Biobank. *Scientific Reports*, 13(1):9221, 2023. doi: 10.1038/s41598-023-36214-0.
- Scott M. Lundberg and Su-In Lee. A unified approach to interpreting model predictions, 2017. URL <https://shap.readthedocs.io/>. Accessed: 2024-08-08.
- Scott M. Lundberg, Gabriel Erion, Hugh Chen, Alex DeGrave, Jordan M. Penttil, Leona Bala, Nair, Ronit Katz, Jonathan Himmelfarb, Nisha Bansal, and

Su-In Lee. From local explanations to global understanding with explainable ai for trees. *Nature Machine Intelligence*, 2(1):2522–5839, 2020.

Rupert W. Major, David Shepherd, Jonathan F. Medcalf, Gang Xu, Laura J. Gray, and Nigel J. Brunskill. The kidney failure risk equation for prediction of end stage renal disease in uk primary care: An external validation and clinical impact projection cohort study. *PLOS Medicine*, 16(11):e1002955, 2019. doi: 10.1371/journal.pmed.1002955. URL <https://journals.plos.org/plosmedicine/article?id=10.1371/journal.pmed.1002955>.

Luke Merrick and Ankur Taly. The explanation game: Explaining machine learning models using shapley values. In *Machine Learning and Knowledge Extraction: 4th IFIP TC 5, TC 12, WG 8.4, WG 8.9, WG 12.9 International Cross-Domain Conference, CD-MAKE 2020, Dublin, Ireland, August 25–28, 2020, Proceedings 4*, pages 17–38. Springer, 2020.

Lloyd S Shapley. A value for n-person games. *Contributions to the Theory of Games*, 2, 1953.

Navdeep Tangri, Morgan E Grams, Andrew S Levey, Josef Coresh, Lawrence J Appel, Brad C Astor, Gabriel Chodick, Allan J Collins, Ognjenka Djurdjev, C Raina Elley, et al. Multinational assessment of accuracy of equations for predicting risk of kidney failure: a meta-analysis. *Jama*, 315(2): 164–174, 2016.

Jing Xiao, Ruifeng Ding, Xiulin Xu, Haochen Guan, Xinhui Feng, Tao Sun, Sibao Zhu, and Zhibin Ye. Comparison and development of machine learning tools in the prediction of chronic kidney disease progression. *Journal of Translational Medicine*, 17(1):119, 2019. doi: 10.1186/s12967-019-1860-0.

Huizhen Ye, Youyuan Chen, Peiyi Ye, Yu Zhang, Xiaoyi Liu, Guanqing Xiao, Zhe Zhang, Yaozhong Kong, and Gehao Liang. Nomogram predicting the risk of three-year chronic kidney disease adverse outcomes among east asian patients with ckd. *BMC Nephrology*, 22(1):322, 2021. doi: 10.1186/s12882-021-02496-7.

## Appendix A. Pipeline Schematic

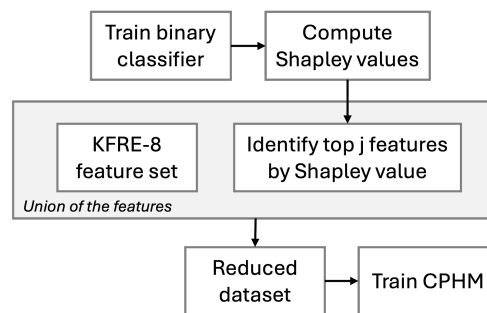


Figure 1: High-level overview of the model pipeline, including ML feature selection and augmented Cox proportional hazards models.

## Appendix B. Related Work

Numerous studies have focused on predicting the outcomes of CKD and its progression. The existing literature documents a variety of methods for developing predictive models, and identification of novel predictors yielding reasonable levels of accuracy, sensitivity, and specificity.

Xiao et al. (2019) assessed the utility of ML models, including logistic regression, Elastic Net, and ensemble methods, to predict 24-hour urinary protein outcomes in CKD patients with proteinuria. Logistic regression emerged as the top performer with an AUC of 0.873, followed closely by linear models such as Elastic Net, lasso, and ridge regression. Bai et al. (2022) compared logistic regression, naïve Bayes, random forest, decision tree, and K-nearest neighbors for predicting ESRD over five years. Random forest achieved the best AUC of 0.81, outperforming the KFRE in sensitivity.

Classical statistical techniques have also been applied to conduct nuanced survival analysis, as demonstrated in the methodology employed by Ye et al. (2021). Ye et al. (2021) utilized Cox proportional hazards regression to develop a nomogram predicting three-year adverse outcomes for East Asian CKD patients, achieving high C-statistics across datasets. The nomogram’s utility was demonstrated via decision curve analysis (DCA), showing a higher net benefit compared to using estimated glomerular filtration rate (eGFR) alone, especially near threshold probabilities where clinical decisions are highly critical.

Leveraging a combined methodology integrating both ML for enhanced feature selection and classical

statistical techniques for survival analysis, Liu et al. (2023) innovated an improved pipeline for predicting breast cancer in post-menopausal women. The method began with the use of the extreme gradient boosting (XGBoost) algorithm to identify novel predictors from over 1,700 features recorded in the UK Biobank, ranking feature importance and highlighting key relationships with Shapley Additive explanations (SHAP) values. The integration of ML in this feature selection process was intended as a strategy to enhance identification of non-linear relationships among predictor features and effectively manage the high-dimensional data. Following feature selection, the researchers constructed two Cox proportional hazards models: a baseline model incorporating known risk factors and polygenic risk scores (PRS), and an augmented model including an additional set of ten novel predictor features identified by XGBoost. The findings demonstrated that the augmented Cox model showed improved predictive performance compared to the baseline model, achieving higher Harrell’s C-index scores.

## Appendix C. Kidney Failure Risk Equation

The KFRE is a predictive tool used to estimate the likelihood of a CKD patient progressing to ESRD typically within a 2 to 5 year time frame (Tangri et al., 2016). These equations have been validated across various populations globally, and have shown to effectively aid clinical decision-making, particularly with regard to determining the timing of treatment interventions such as dialysis or transplantation (Major et al., 2019).

The KFRE is available in both 4-variable (KFRE-4) and 8-variable model (KFRE-8) versions (Foundation, 2023). KFRE-4 makes use of age, sex, eGFR, and urine albumin-to-creatinine ratio (UACR). KFRE-8 includes these same factors as KFRE-4 with the addition of serum calcium, serum phosphorus, serum bicarbonate, and serum albumin.

## Appendix D. Binary Classifier

Let  $\tau \in \mathbb{R}$  be a threshold value, and let  $f(\cdot; \theta) : \mathbb{R}^n \mapsto \{0, 1\}$  represent a function parameterized by  $\theta$ . For a data sample  $\mathbf{x}_i \in \mathbb{R}^n$ , a binary classifier assigns a

label  $\hat{y}_i$  based on  $\tau$  as,

$$\hat{y}_i = \begin{cases} 0, & f(\mathbf{x}_i; \theta) < \tau, \\ 1, & f(\mathbf{x}_i; \theta) \geq \tau. \end{cases} \quad (1)$$

The function  $f(\cdot; \theta)$  can be represented by a variety of machine learning models. In this paper, we focus on tree-based methods D.2, linear models D.1, and deep learning approaches D.3, each capable of performing binary classification as defined in equation (1).

### D.1. Linear models

**Logistic regression.** Logistic regression is a fundamental statistical modeling technique used to estimate the probability of a binary outcome, based on one or more predictor variables (Hosmer et al., 2013). Let  $\mathbf{x}_i \in \mathbb{R}^{n_0}$  represent input features and  $\mathbf{w} \in \mathbb{R}^{n_0}$  denote a vector of coefficients to be learned. The probability of the binary event occurring  $y_i \in \{0, 1\}$  for the  $i$ -th data sample, is defined as

$$\hat{y}_i = \sigma(\mathbf{w}^T \mathbf{x}_i + b). \quad (2)$$

### D.2. Tree-based methods

**Decision tree.** A decision tree is a non-parametric supervised learning algorithm that recursively partitions the input space based on feature values, forming a tree structure composed of decision nodes and leaf nodes, where each leaf node assigns a predicted class label (Breiman et al., 1984). The prediction for a data point is given by

$$\hat{y}_i = \sum_{l=1}^L p_l \mathbb{I}\{\mathbf{x}_i \in R_l\} \quad (3)$$

where  $p_l$  is the predicted class probability for region  $R_l$ , and  $\mathbb{I}\{\mathbf{x}_i \in R_l\}$  is an indicator function that equals 1 if the sample  $\mathbf{x}_i$  falls into region  $R_l$ , and 0 otherwise.

**Random forest.** A random forest is an ensemble learning method, aggregating multiple decision trees leads to improve model robustness and generalization (Breiman, 2001). For binary classification, the prediction  $\hat{y}_i$  for a given data point  $\mathbf{x}_i \in \mathbb{R}^{n_0}$  is obtained by aggregating the predictions from  $T$  individual decision trees in the forest

$$\hat{y}_i = \frac{1}{T} \sum_{t=1}^T \hat{y}_i^{(t)} \quad (4)$$

Here,  $\hat{y}_i^{(t)}$  denotes the prediction from the  $t$ -th decision tree.

**Extreme gradient boosting.** Extreme Gradient Boosting (XGBoost) is a scalable and efficient ML algorithm, effectively enhancing model accuracy through the combination of multiple weak learners [Chen and Guestrin \(2016\)](#). The prediction for a data sample  $i$  can be expressed as the weighted sum of the outputs from  $K$  decision trees

$$\hat{y}_i = \sum_{k=1}^K f_k(\mathbf{x}_i) \quad (5)$$

where  $f_k$  denotes the  $k$ -th tree’s contribution, and  $\mathbf{x}_i \in \mathbb{R}^{n_0}$  represents the input features of sample  $i$ . The ensemble of trees allows the model to capture complex non-linear patterns, much like the layers in a neural network.

### D.3. Neural networks

**Fully-connected neural network.** A fully connected neural network can be defined as

$$\hat{y}_i = \sigma(W_L(\sigma(W_{L-1}(\cdots \sigma(W_1 \mathbf{x}_i + \mathbf{b}_1) \cdots) + \mathbf{b}_{L-1}) + \mathbf{b}_L)) \quad (6)$$

where  $W_l \in \mathbb{R}^{n_l \times n_{l-1}}$  and  $\mathbf{b}_l \in \mathbb{R}^{n_l}$  represent the weights and biases for each layer  $l \in \{1, 2, \dots, L\}$ , and  $\sigma$  is an activation function such as the rectified linear unit (ReLU) [\(LeCun et al., 2015\)](#). The input vector  $\mathbf{x}_i \in \mathbb{R}^{n_0}$  represents the features for data sample  $i$ , and the output  $\hat{y}_i$  is the predicted label. The activation function  $\sigma$  introduces non-linearity, enabling the network to model complex patterns.

**Residual neural network.** A ResNet addresses the degradation problem in excessively deep networks, wherein added depth increases training error, through the introduction of shortcut connections [\(He et al., 2016\)](#). The output of a residual block can be defined as

$$\mathbf{y}_i = F(\mathbf{x}_i, \{W_i\}) + \mathbf{x}_i \quad (7)$$

where  $\mathbf{x}_i \in \mathbb{R}^{n_0}$  is the input vector for data sample  $i$ , and  $\mathbf{y}_i$  is the output of the residual block. The function  $F$  consists of weights  $\{W_i\}$  where  $W_i \in \mathbb{R}^{n_i \times n_{i-1}}$ , as well as the biases and activation functions for each layer  $l$  across the respective layers within the block [\(6\)](#), representing the residual mapping. The addition of the input  $\mathbf{x}_i$  to the output of  $F$  characterizes a shortcut connection, allowing gradients to flow directly through the network with no additional computational complexity or training error degradation.

To align the dimensions of  $\mathbf{x}_i$  with those of  $F(\mathbf{x}_i, \{W_i\})$ , a linear transformation  $W_s$  may be applied to  $\mathbf{x}_i$

$$\mathbf{y}_i = F(\mathbf{x}_i, \{W_i\}) + W_s \mathbf{x}_i \quad (8)$$

where  $W_s \in \mathbb{R}^{n_i \times n_0}$ .

## Appendix E. Shapley values

Shapley values are a concept from cooperative game theory providing a fair way to distribute total gains or cost amongst multiple players in a coalition [\(Shapley, 1953\)](#). Let  $M = \{1, \dots, m\}$  represent a set of players taking part in a game  $\nu : 2^M \mapsto \mathbb{R}$ . The game,  $\nu$  is a characteristic function returning a scalar reward for each coalition  $A \subseteq M$ . It is assumed that  $\nu(\emptyset) = 0$ . The Shapley value of a player  $k$  can be computed by

$$\phi_k = \sum_{A \subseteq M \setminus \{k\}} \frac{(m - |A| - 1)! |A|!}{m!} (\nu(A \cup \{k\}) - \nu(A)). \quad (9)$$

Here  $|\cdot|$  represents cardinality. Shapley values are commonly used in explainable machine learning [\(Merrick and Taly, 2020\)](#). In the context of machine learning, each feature  $x_i$  in a feature vector  $\mathbf{x} \in \mathbb{R}^n$  is considered as the player. While the output from a trained model  $f : \mathbb{R}^n \mapsto \mathbb{R}$  is considered to be reward  $\nu$ . As a result,  $\phi_i$  measures the  $x_i$ -th feature’s importance with respect to model output.

## Appendix F. Cox proportional hazards model

The CPHM is a statistical technique used for modeling the time-dependent risk of an event occurring, often applied in survival analysis [\(Cox, 1972\)](#). Let  $\mathbf{x} \in \mathbb{R}^d$  represent a feature vector of  $d$ -dimension and let  $\beta \in \mathbb{R}^d$  denote a corresponding vector of coefficients. The CPHM is based on a hazard function, defined by

$$\lambda(t | \mathbf{x}) = \lambda_0(t) \exp(\beta^T \mathbf{x}). \quad (10)$$

Here  $\lambda_0(\cdot) : \mathbb{R}^+ \mapsto \mathbb{R}^+$  is the baseline hazard function, representing the hazard rate when  $\mathbf{x} = 0$ . The baseline hazard function  $\lambda_0(\cdot)$  is unspecified, allowing for a semi-parametric approach where the effect of the  $\mathbf{x}$  is modeled parametrically through  $\beta$ , while the baseline hazard can vary non-parametrically over time. This flexibility makes the CPHM a powerful tool for survival analysis, as it does not assume a specific distribution for the survival times.



**Partial likelihood.** The parameters  $\beta$  are estimated using the method of partial likelihood, which focuses on the order of events rather than their exact timing. The partial likelihood function  $L(\beta)$  is given by

$$L(\beta) = \prod_{i=1}^D \frac{\exp(\beta^T x_i)}{\sum_{j \in R(t_i)} \exp(\beta^T x_j)}, \quad (11)$$

where  $D$  is the number of observed events, and  $R(t_i)$  is the risk set at time  $t_i$ , consisting of all individuals who are at risk just prior to time  $t_i$ . The partial likelihood function is maximized to obtain the estimates of  $\beta$ .

## Appendix G. Evaluation Metrics

### G.1. Area under the receiver operating characteristic curve.

The AUROC is a metric for evaluating the performance of binary classification models. It measures the ability of a model to distinguish between positive and negative classes by plotting the true positive rate against the false positive rate across various decision thresholds. AUROC score ranges from 0 to 1, where 1 indicates perfect discrimination, 0.5 represents random guessing. In survival analysis, a time-dependent version of the AUROC is often applied to evaluate predictive accuracy at different time points.

### G.2. Concordance index.

The C-index is a metric for evaluating the predictive accuracy of survival models, assessing how well the predicted and actual order of events agree (Harrell et al., 1982). Let  $T$  denote the event time, C-index is then defined by,

$$C = \frac{\sum_{i,j} \mathbb{1}[T_i < T_j] \mathbb{1}[\hat{T}_i < \hat{T}_j] \delta_i}{\sum_{i,j} \mathbb{1}[T_i < T_j] \delta_i}. \quad (12)$$

Here,  $\delta_i = 1$  if the event time  $T_i$  is observed (i.e. not censored), and  $\delta_i = 0$  otherwise. C-index is a generalisation of the AUROC. A C-index of 1 indicates perfect predictions and 0 represents the worst performance.

### G.3. Brier score.

The Brier score is a metric used to evaluate the accuracy of probabilistic predictions in survival analysis (Brier, 1950). It measures the weighted mean squared

difference between the predicted probabilities and the actual outcomes. Brier score at time  $t$  is defined by,

$$\mathcal{B}(t) = \frac{1}{N} \sum_{i=1}^N \left( \mathbb{1}[T_i > t] - \hat{S}(t|\mathbf{x}_i) \right)^2, \quad (13)$$

where  $\hat{S}(\cdot)$  represents a predicted survival function. The Brier score ranges from 0 to 1, with 0 indicating perfect accuracy and 1 representing the worst accuracy.

## Appendix H. Supplementary Tables

### H.1. Data characteristics

Table 1: CKD-related ICD-9 codes in MIMIC-IV

ICD-9 Code	Long Title
5851	Chronic kidney disease, Stage I
5852	Chronic kidney disease, Stage II (mild)
5853	Chronic kidney disease, Stage III (moderate)
5854	Chronic kidney disease, Stage IV (severe)
5855	Chronic kidney disease, Stage V
5856	End stage renal disease
5859	Chronic kidney disease, unspecified

Table 2: Input categories of the 1,373 input features used in ML feature selection.

Input Category	Frequency
Patient Demographics	6 (0.44%)
CKD Diagnostic Information	3 (0.22%)
Clinical Lab Data	444 (32.34%)
Comorbid Health Conditions	921 (67.08%)

### H.2. Hyperparameters

Table 3: Manually selected hyperparameter values for FCNN and ResNet.

Hyperparameter	FCNN	ResNet
learning_rate	0.001	0.001
weight_decay	$1 \times 10^{-4}$	$1 \times 10^{-4}$
max_epochs	35	30
early_stopping	8	5

Table 4: Optimized hyperparameter values and search spaces for Bayesian optimization.

Hyperparameter	XGBoost	RF	DT	LR
max_depth	14 (5 – 20)	33 (2 – 50)	6 (1 – 50)	NA
min_samples_split	NA	6 (2 – 20)	6 (2 – 20)	NA
min_samples_leaf	NA	7 (1 – 20)	11 (1 – 20)	NA
n_estimators	83 (50 – 150)	138 (50 – 200)	NA	NA
min_child_weight	1 (1 – 10)	NA	NA	NA
gamma	2.61 (0.5 – 3.0)	NA	NA	NA
subsample	0.78 (0.6 – 1.0)	NA	NA	NA
colsample_bytree	0.76 (0.6 – 1.0)	NA	NA	NA
colsample_bylevel	0.56 (0.01 – 0.6)	NA	NA	NA
learning_rate	0.22 (0.01 – 0.3)	NA	NA	NA
c	NA	NA	NA	0.095 (0.01 – 1.0)

### H.3. Model performance

Table 5: AUROC scores for models used for feature extraction.

Model	AUC-ROC Avg.	AUC-ROC Best
XGBoost	<b><math>0.7796 \pm 0.0257</math></b>	0.8105
LR	$0.7027 \pm 0.0230$	<b>0.7268</b>
DT	$0.7283 \pm 0.0364$	<b>0.7799</b>
RF	$0.5796 \pm 0.0092$	<b>0.5905</b>
FCNN	$0.6612 \pm 0.0179$	<b>0.6916</b>
ResNet	$0.6540 \pm 0.0090$	<b>0.6661</b>

Table 6: Comparison of Cox proportional hazards models based on C-Index scores obtained from five-fold cross-validation.

Model	C-Index Avg.	C-Index Best
Baseline Cox	$0.8820 \pm 0.0082$	0.8910
XGBoost-Augmented Cox	$0.8876 \pm 0.0071$	0.8929
LR-Augmented Cox	<b><math>0.8900 \pm 0.0092</math></b>	0.9016
DT-Augmented Cox	$0.8855 \pm 0.0051$	0.8901
RF-Augmented Cox	$0.8865 \pm 0.0082$	0.8936
FCNN-Augmented Cox	$0.8873 \pm 0.0073$	0.8942
ResNet-Augmented Cox	$0.8878 \pm 0.0073$	0.8930

Table 7: Comparison of Cox proportional hazards models based on Brier scores at 1-5 year time intervals.

Model	1 Year	2 Year	3 Year	4 Year	5 Year
Baseline Cox	0.0321	0.0581	0.0730	0.0901	0.1120
XGBoost-Augmented Cox	<b>0.0289</b>	0.0506	0.0673	<b>0.0750</b>	<b>0.0801</b>
LR-Augmented Cox	0.0308	0.0550	0.0673	0.0830	0.1033
DT-Augmented Cox	0.0309	0.0496	0.0646	0.0841	0.1010
RF-Augmented Cox	0.0321	0.0590	0.0732	0.0899	0.1077
FCNN-Augmented Cox	0.0299	<b>0.0485</b>	<b>0.0625</b>	0.0828	0.0988
ResNet-Augmented Cox	0.0321	0.0572	0.0710	0.0852	0.1079

Table 8: Comparison of Cox proportional hazards models based on AUC scores at 1-5 year time intervals.

Model	1 Year	2 Year	3 Year	4 Year	5 Year
Baseline Cox	0.9551	0.9369	0.9357	0.9212	0.9113
XGBoost-Augmented Cox	0.9494	0.9171	0.9071	<b>0.9376</b>	<b>0.9507</b>
LR-Augmented Cox	<b>0.9634</b>	<b>0.9499</b>	<b>0.9453</b>	0.9300	0.9234
DT-Augmented Cox	0.9340	0.9494	0.9407	0.9090	0.9111
RF-Augmented Cox	0.9472	0.9426	0.9399	0.9212	0.9149
FCNN-Augmented Cox	0.9364	0.9466	0.9422	0.9169	0.9149
ResNet-Augmented Cox	0.9449	0.9423	0.9419	0.9266	0.9167

### H.4. Feature selection

Table 9: Hazard ratios, 95% confidence intervals (CI), and p-values for XGBoost-augmented Cox model.

Features	Hazard Ratio (95% CI)	p-value
Creatinine_mean	1.0995 (0.9403, 1.2856)	0.2345
Creatinine_max	0.9807 (0.9436, 1.0193)	0.3228
Renal dialysis status	1.7696 (1.4469, 2.1644)	$2.77 \times 10^{-8}$
Creatinine_last	1.0287 (0.9807, 1.0790)	0.2455
Creatinine_median	0.8753 (0.7823, 0.9794)	0.0202
Urea_Nitrogen_max	1.0031 (1.0002, 1.0060)	0.0371
Potassium_max	1.0790 (0.8686, 1.3403)	0.4920
Creatinine_Urine_min	0.9979 (0.9958, 1.0001)	0.0644
Urea_Nitrogen_last	0.9978 (0.9945, 1.0011)	0.1864
Unspecified essential hypertension	0.5960 (0.5211, 0.6817)	$4.28 \times 10^{-14}$
Orthostatic hypotension	1.1601 (0.9631, 1.3976)	0.1179
White_Blood_Cells_min	0.9822 (0.9446, 1.0212)	0.3655
Bilirubin_Total_mean	1.0254 (0.9757, 1.0777)	0.3219
Protein/Creatinine_Ratio_max	0.9892 (0.9804, 0.9980)	0.0168
Neutrophils_max	0.9964 (0.9882, 1.0046)	0.3833
Platelet_Count_median	1.0007 (0.9994, 1.0020)	0.2853
Hemoglobin_max_y	0.8836 (0.8473, 0.9214)	$7.34 \times 10^{-9}$
Eosinophils_first	1.0253 (1.0044, 1.0466)	0.0176
Cholesterol_Total_last	0.9999 (0.9984, 1.0014)	0.9190
MCHC_min	1.0058 (0.9567, 1.0573)	0.8222
Urea_Nitrogen_first	1.0018 (0.9977, 1.0058)	0.3903
Glucose_min	0.9971 (0.9944, 0.9999)	0.0391
Creatinine_min	1.3787 (1.2236, 1.5535)	$1.34 \times 10^{-7}$
Uric_Acid_first	1.0220 (0.9897, 1.0553)	0.1844
Acute kidney failure, unspecified	1.0080 (0.8587, 1.1833)	0.9226
Total Protein_Urine_last	1.0007 (1.0001, 1.0013)	0.0262
Mitral valve disorders	0.9100 (0.7684, 1.0777)	0.2747
Potassium_mean	0.7925 (0.5992, 1.0480)	0.1028
Protein/Creatinine_Ratio_last	1.0288 (1.0099, 1.0480)	0.0027
Platelet_Count_max	0.9994 (0.9988, 1.0001)	0.0960
MCH_max	1.0056 (0.9814, 1.0304)	0.6525
marital_status_MARRIED	0.9824 (0.8686, 1.1110)	0.7772
Sodium_last	1.0026 (0.9874, 1.0181)	0.7382
Anemia, unspecified	0.9008 (0.7920, 1.0245)	0.1116
Creatinine_Urine_last	1.0006 (0.9991, 1.0021)	0.4252
Asparate_Aminotransferase (AST)_first	0.9993 (0.9985, 1.0002)	0.1381
Globulin_last	0.9332 (0.8227, 1.0585)	0.2819
Urea_Nitrogen_median	1.0090 (1.0030, 1.0150)	0.0031
White_Blood_Cells_mean	1.0057 (0.9855, 1.0264)	0.5813
Eosinophils_max	0.9933 (0.9805, 1.0063)	0.3133

Table 10: Hazard ratios, 95% confidence intervals (CI), and p-values for FCNN-augmented Cox model.

Features	Hazard Ratio (95% CI)	p-value
Renal dialysis status	1.805 (1.465, 2.224)	$2.92 \times 10^{-8}$
Coronary atherosclerosis of native coronary artery	0.972 (0.8548, 1.117)	0.6876
Creatinine_last	1.021 (0.9729, 1.071)	0.4013
Anemia, unspecified	0.9664 (0.8501, 1.099)	0.6012
race_WHITE	1.014 (0.8864, 1.160)	0.8418
Other and unspecified hyperlipidemia	0.9728 (0.8472, 1.117)	0.6952
Unspecified essential hypertension	0.5962 (0.5204, 0.6830)	$8.75 \times 10^{-14}$
MCHC_min	1.045 (0.9899, 1.102)	0.1117
Chloride_max	1.012 (0.9944, 1.030)	0.1837
marital_status_SINGLE	1.144 (0.9956, 1.313)	0.0577
Urea_Nitrogen_median	1.003 (0.9897, 1.016)	0.6907
Potassium_min	0.8744 (0.6962, 1.098)	0.2484
Urea_Nitrogen_mean	1.013 (0.9949, 1.031)	0.1625
Long-term use of other medications	0.7729 (0.6029, 0.9908)	0.0420
Creatinine_min	1.297 (1.156, 1.455)	$9.91 \times 10^{-6}$
Urea_Nitrogen_last	0.9984 (0.9951, 1.002)	0.3435
Platelet_Count_last	1.0003 (0.9997, 1.0009)	0.3399
Acute kidney failure, unspecified	1.080 (0.9205, 1.267)	0.3456
Urea_Nitrogen_min	1.004 (0.9945, 1.014)	0.4104
Urea_Nitrogen_first	1.001 (0.9970, 1.0045)	0.7037
Personal history of TIA and cerebral infarction without residual deficits	0.9398 (0.8046, 1.098)	0.4334
Urea_Nitrogen_max	1.001 (0.9970, 1.0046)	0.6792
Neutrophils_min	0.9928 (0.9837, 1.0019)	0.1194
Diabetes with renal manifestations	0.9806 (0.8457, 1.137)	0.7954
MCHC_max	0.9086 (0.8559, 0.9645)	0.0017
Peripheral vascular disease, unspecified	0.9203 (0.7872, 1.076)	0.2974
Surgical operation with transplant causing abnormal reaction	1.069 (0.8494, 1.345)	0.5694
White_Blood_Cells_min	0.9918 (0.9601, 1.024)	0.6173
Potassium_max	0.9548 (0.8047, 1.133)	0.5962
Creatinine_Urine_last	0.9994 (0.9981, 1.0006)	0.3338
Percutaneous transluminal coronary angioplasty status	1.032 (0.8793, 1.212)	0.6968
Sodium_first	1.010 (0.9922, 1.028)	0.2764
Creatinine_median	0.9610 (0.8802, 1.049)	0.3753
Hemoglobin_first_y	0.9300 (0.8966, 0.9647)	$1.03 \times 10^{-4}$
Aortic valve disorders	0.8828 (0.7213, 1.080)	0.2266
Lymphocytes_max	0.9934 (0.9835, 1.0034)	0.1944
Other chronic pulmonary heart diseases	1.070 (0.9202, 1.244)	0.3791
Atrial fibrillation	0.9931 (0.8683, 1.136)	0.9194
Creatinine_mean	1.013 (0.9562, 1.074)	0.6561
Urinary tract infection, site not specified	0.8642 (0.7574, 0.9862)	0.0303

Table 11: Hazard ratios, 95% confidence intervals (CI), and p-values for ResNet-augmented Cox model.

Features	Hazard Ratio (95% CI)	p-value
Coronary atherosclerosis of native coronary artery	0.8884 (0.7719, 1.0225)	0.0989
Renal dialysis status	2.0339 (1.6719, 2.4744)	$1.26 \times 10^{-12}$
Creatinine_last	0.9853 (0.9410, 1.0318)	0.5294
MCHC_min	1.0140 (0.9577, 1.0737)	0.6331
Anemia, unspecified	0.9505 (0.8341, 1.0831)	0.4461
Urea_Nitrogen_max	0.9996 (0.9961, 1.0031)	0.8333
marital_status_SINGLE	1.1052 (0.9317, 1.3110)	0.2509
Chloride_max	1.0004 (0.9833, 1.0178)	0.9630
race_WHITE	0.9620 (0.8415, 1.0997)	0.5700
Potassium_min	0.8582 (0.6767, 1.0884)	0.2072
Unspecified essential hypertension	0.6198 (0.5425, 0.7081)	$1.90 \times 10^{-12}$
Urea_Nitrogen_mean	1.0251 (1.0064, 1.0441)	0.0084
Urea_Nitrogen_min	1.0064 (0.9969, 1.0159)	0.1861
Platelet_Count_last	1.0005 (0.9998, 1.0013)	0.1419
Urea_Nitrogen_median	0.9929 (0.9795, 1.0064)	0.3003
Esophageal reflux	0.9256 (0.8159, 1.0500)	0.2295
Other and unspecified hyperlipidemia	1.0613 (0.9205, 1.2236)	0.4128
Potassium_last	1.0092 (0.9676, 1.2485)	0.1459
marital_status_MARRIED	1.0400 (0.8911, 1.2137)	0.6188
MCHC_max	0.9063 (0.8517, 0.9643)	0.0019
Creatinine_Urine_max	0.9996 (0.9987, 1.0006)	0.4338
Monocytes_min	0.9704 (0.9268, 1.0161)	0.2010
Potassium_max	0.9714 (0.8131, 1.1604)	0.7488
Chloride_first	1.0020 (0.9875, 1.0168)	0.7880
Lymphocytes_max	0.9883 (0.9783, 0.9983)	0.0226
Hypertrophy of prostate without urinary obstruction	1.0246 (0.8614, 1.2187)	0.7836
Diabetes mellitus type II, not uncontrolled	0.8598 (0.7569, 0.9767)	0.0202
Peripheral vascular disease, unspecified	0.9851 (0.8448, 1.1487)	0.8478
Percutaneous transluminal coronary angioplasty status	1.0821 (0.9169, 1.2770)	0.3507
Aortic valve disorders	0.8724 (0.7054, 1.0789)	0.2080
Physical restraints status	0.7141 (0.5096, 1.0008)	0.0505
Creatinine_mean	1.0826 (1.0067, 1.1642)	0.0323
Platelet_Count_max	0.9994 (0.9989, 1.0000)	0.0290
Neutrophils_last	1.0063 (1.0000, 1.0126)	0.0494
Neutrophils_max	0.9921 (0.9816, 1.0028)	0.1476
Pure hypercholesterolemia	0.9737 (0.8515, 1.1134)	0.6971
MCV_min	1.0139 (1.0036, 1.0243)	0.0078
Hypovolemia	0.8641 (0.7234, 1.0321)	0.1071
Neutrophils_min	0.9857 (0.9765, 0.9949)	0.0024
Gout, unspecified	0.9369 (0.8115, 1.0818)	0.3747

Table 12: Hazard ratios, 95% confidence intervals (CI), and p-values for LR-augmented Cox model.

Features	Hazard Ratio (95% CI)	p-value
Renal dialysis status	2.0084 (1.6313, 2.4728)	$4.99 \times 10^{-11}$
Creatinine_last	0.9998 (0.9538, 1.0480)	0.9935
Urea_Nitrogen_mean	1.0154 (1.0069, 1.0240)	0.00036
MCHC_min	1.0939 (1.0341, 1.1572)	0.0018
MCHC_max	1.0058 (0.9336, 1.0837)	0.8784
Protein_mean	1.0013 (1.0006, 1.0020)	0.00053
Cholesterol_Ratio. (Total/HDL)_first	1.0189 (0.9661, 1.0746)	0.4899
Nucleated_Red_Cells_Last	1.0078 (1.0001, 1.0155)	0.0460
Eosinophils_mean	1.0327 (0.7883, 1.3530)	0.8153
Chloride_max	0.9987 (0.9789, 1.0190)	0.9009
Unspecified essential hypertension	0.5907 (0.5172, 0.6747)	$8.35 \times 10^{-15}$
Protein_Total_last	1.1584 (0.9418, 1.4249)	0.1640
Chloride_last	1.0061 (0.9912, 1.0211)	0.4251
Urea_Nitrogen_last	0.9992 (0.9950, 1.0026)	0.6607
Protein_Total_max	0.8192 (0.6546, 1.0252)	0.0814
Cholesterol_HDL_last	0.9975 (0.9923, 1.0027)	0.3405
Cholesterol_Total_first	0.9984 (0.9966, 1.0003)	0.0932
Uric_Acid_median	1.0217 (0.9822, 1.0628)	0.2853
Urea_Nitrogen_max	1.0005 (0.9973, 1.0037)	0.7593
MCHC_mean	0.8499 (0.7670, 0.9417)	0.0019
Other and unspecified hyperlipidemia	0.9549 (0.8326, 1.0951)	0.5089
marital_status_SINGLE	1.1004 (0.9573, 1.2650)	0.1784
MCV_mean	1.0363 (1.0024, 1.0715)	0.0357
Sodium_mean	0.9867 (0.9545, 1.0199)	0.4275
Anemia, unspecified	0.9385 (0.8235, 1.0694)	0.3406
Atrial fibrillation	0.9819 (0.8596, 1.1214)	0.7872
Severe sepsis	0.8669 (0.7257, 1.0357)	0.1156
Creatinine_median	1.0763 (1.0056, 1.1519)	0.0339
Creatinine_first	0.9238 (0.8646, 0.9871)	0.0190
Myelocytes_mean	1.0185 (0.9054, 1.1457)	0.7602
Creatinine_Urine_last	1.0002 (0.9990, 1.0014)	0.7027
Neutrophils_min	0.9975 (0.9927, 1.0024)	0.3178
Diabetes with renal manifestations, type II or unspecified type	0.8890 (0.7646, 1.0336)	0.1261
Protein_Total_first	0.9964 (0.8087, 1.2276)	0.9727
Globulin_last	1.1550 (0.9877, 1.3507)	0.0710
Urea_Nitrogen_min	1.0090 (0.9994, 1.0186)	0.0660
Cholesterol_LDL_Calculated_median	1.0027 (1.0000, 1.0053)	0.0458
Monocytes_min	0.9893 (0.9453, 1.0353)	0.6425
Neutrophils_max	0.9973 (0.9877, 1.0070)	0.5862
Protein_Total_min	0.9026 (0.7470, 1.0907)	0.2887

Table 13: Hazard ratios, 95% confidence intervals (CI), and p-values for DT-augmented Cox model.

Features	Hazard Ratio (95% CI)	p-value
Creatinine_max	0.9517 (0.9167, 0.9880)	0.0095
Renal dialysis status	1.8287 (1.5099, 2.2148)	$6.58 \times 10^{-10}$
Creatinine_mean	1.2372 (1.0643, 1.4383)	0.0056
Creatinine_last	1.0405 (0.9948, 1.0884)	0.0834
Creatinine_median	0.9259 (0.8307, 1.0320)	0.1641
RBC_max	1.0001 (0.9996, 1.0007)	0.6106
Urea_Nitrogen_max	0.9988 (0.9956, 1.0020)	0.4569
Protein_first	1.0010 (1.0005, 1.0014)	$3.77 \times 10^{-5}$
Monocytes_first	1.0064 (0.9816, 1.0319)	0.6162
Platelet_Count_first	0.9996 (0.9989, 1.0003)	0.2354
Diabetes with other specified manifestations	0.9198 (0.7790, 1.0861)	0.3241
Uric_Acid_max	0.9793 (0.9481, 1.0116)	0.2065
Acute kidney failure, unspecified	1.0816 (0.9249, 1.2649)	0.3257
Urea_Nitrogen_mean	1.0217 (1.0151, 1.0284)	$1.26 \times 10^{-10}$
MCHC_mean	0.9559 (0.9003, 1.0149)	0.1399
Pure hypercholesterolemia	0.8793 (0.7736, 0.9995)	0.0491
Absolute_Lymphocyte_Count_Last	0.8964 (0.7646, 1.0510)	0.1780
Alanine_Aminotransferase (ALT)_median	0.9991 (0.9980, 1.0002)	0.0982
Other musculoskeletal symptoms	0.9351 (0.7290, 1.1995)	0.5974
Cholesterol_Ratio.(Total/HDL)_last	1.0376 (0.9962, 1.0807)	0.0755
Glucose_mean	0.9964 (0.9945, 0.9984)	$3.11 \times 10^{-4}$
Platelet_Count_last	1.0001 (0.9995, 1.0008)	0.6477
Reticulocyte_Count_Manual_min	1.0371 (0.9430, 1.1405)	0.4533

## Appendix I. Mean Absolute SHAP Values

Table 14: Hazard ratios, 95% confidence intervals (CI), and p-values for RF-augmented Cox model.

Features	Hazard Ratio (95% CI)	p-value
Urea_Nitrogen_max	0.9990 (0.9956, 1.0024)	0.5460
Creatinine_max	0.9083 (0.8654, 0.9533)	$9.81 \times 10^{-5}$
Creatinine_last	1.0238 (0.9762, 1.0738)	0.3323
Creatinine_mean	1.5034 (1.2271, 1.8420)	$8.31 \times 10^{-5}$
Renal_dialysis_status	2.1128 (1.7321, 2.5771)	$1.58 \times 10^{-13}$
Creatinine_median	0.8243 (0.7081, 0.9596)	0.0127
Potassium_max	0.9503 (0.8078, 1.1178)	0.5382
Urea_Nitrogen_mean	1.0280 (1.0106, 1.0456)	0.0015
Protein/Creatinine_Ratio_last	1.0250 (0.9944, 1.0567)	0.1108
Eosinophils_max	0.9956 (0.9831, 1.0082)	0.4928
Creatinine_Urine_min	0.9995 (0.9976, 1.0014)	0.5852
Total_Protein_Urine_mean	0.9973 (0.9923, 1.0022)	0.2794
MCHC_min	1.0139 (0.9657, 1.0645)	0.5788
Protein/Creatinine_Ratio_median	1.1237 (0.9762, 1.2936)	0.1043
Total_Protein_Urine_max	0.9997 (0.9985, 1.0009)	0.6200
Hemoglobin_min_y	0.9747 (0.9311, 1.0204)	0.2731
Protein/Creatinine_Ratio_mean	0.9218 (0.7635, 1.1128)	0.3965
Uric_Acid_mean	0.9381 (0.7166, 1.2280)	0.6419
Total_Protein_Urine_median	1.0014 (0.9983, 1.0045)	0.3690
Acute_kidney_failure_unspecified	1.0813 (0.9225, 1.2673)	0.3348
Protein/Creatinine_Ratio_max	0.9969 (0.9587, 1.0367)	0.8782
Urea_Nitrogen_Urine_min	1.0001 (0.9995, 1.0007)	0.7437
Protein_mean	1.0020 (1.0008, 1.0032)	0.0014
Urea_Nitrogen_median	0.9950 (0.9816, 1.0086)	0.4723
Asparate_Aminotransferase (AST)_min	0.9996 (0.9982, 1.0010)	0.5581
Total_Protein_Urine_last	1.0005 (0.9995, 1.0016)	0.3179
Protein_max	0.9994 (0.9988, 1.0000)	0.0632
Uric_Acid_max	0.9566 (0.8956, 1.0218)	0.1875
Uric_Acid_median	1.1060 (0.8992, 1.3604)	0.3402
Protein/Creatinine_Ratio_first	1.0372 (0.8954, 1.0917)	0.1620
Total_Protein_Urine_first	1.0009 (0.9996, 1.0021)	0.1653
Total_Protein_Urine_min	1.0013 (0.9992, 1.0034)	0.2300
Chloride_min	1.0189 (1.0048, 1.0333)	0.0085
Protein_last	0.9996 (0.9989, 1.0002)	0.1891
Uric_Acid_last	1.0389 (0.9678, 1.1151)	0.2912
Albumin_Urine_max	0.9989 (0.9969, 1.0010)	0.3093
Neutrophils_min	0.9978 (0.9930, 1.0025)	0.3541
Protein/Creatinine_Ratio_min	0.9316 (0.8552, 1.0147)	0.1042
Urea_Nitrogen_Urine_last	0.9995 (0.9989, 0.9999)	0.0437
Albumin_Urine_last	1.0005 (0.9981, 1.0029)	0.6867

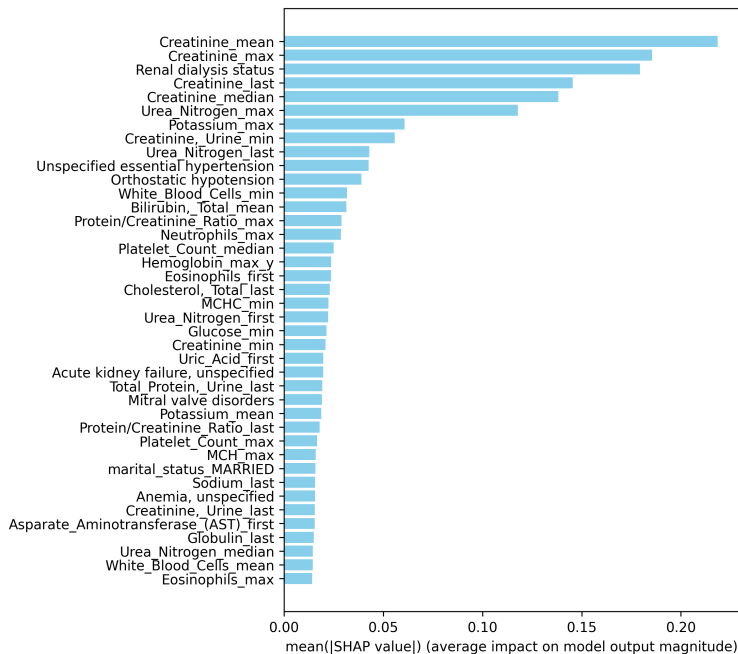


Figure 2: Top 40 mean absolute SHAP values from XGboost model.

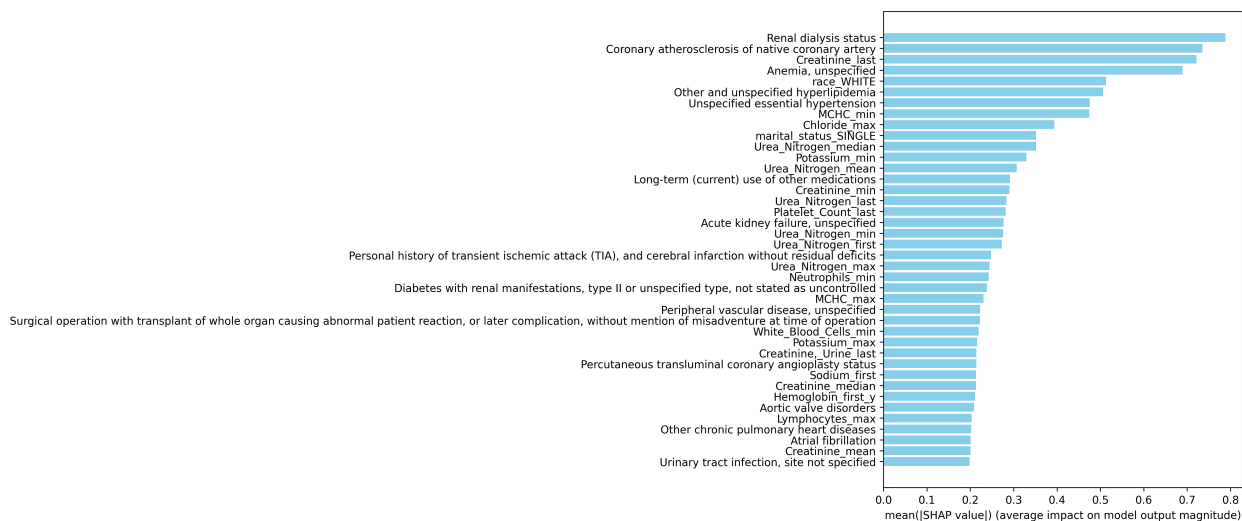


Figure 3: Top 40 mean absolute SHAP values from FCNN model.

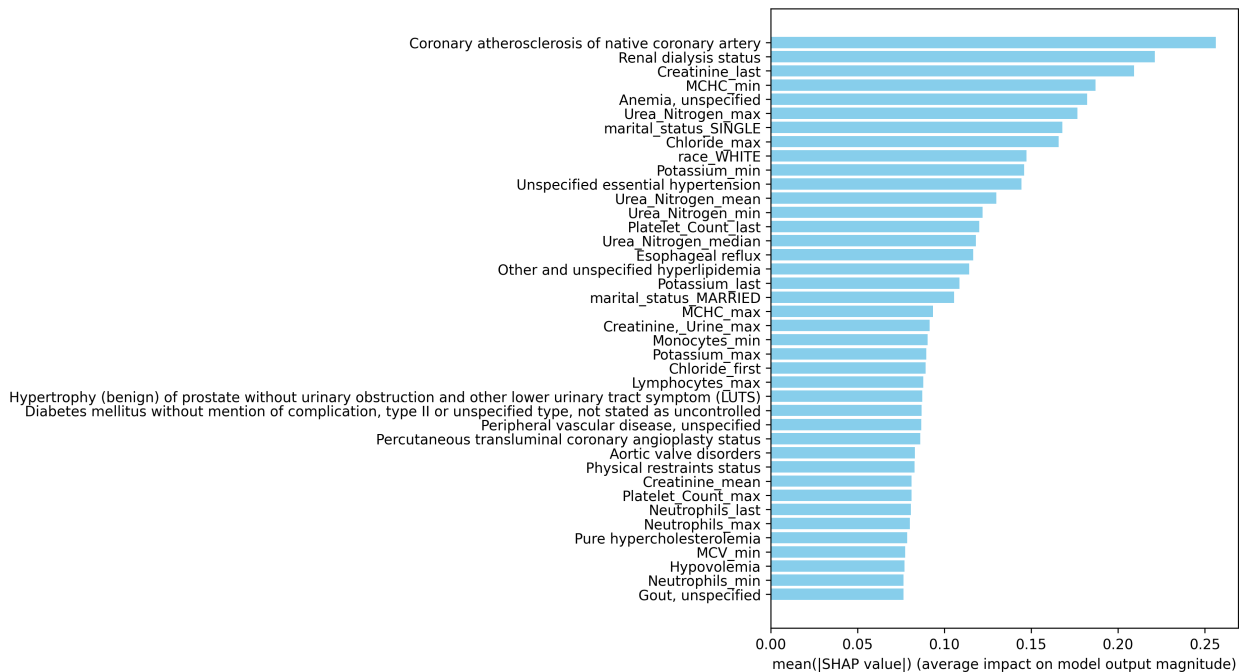


Figure 4: Top 40 mean absolute SHAP values from ResNet model.

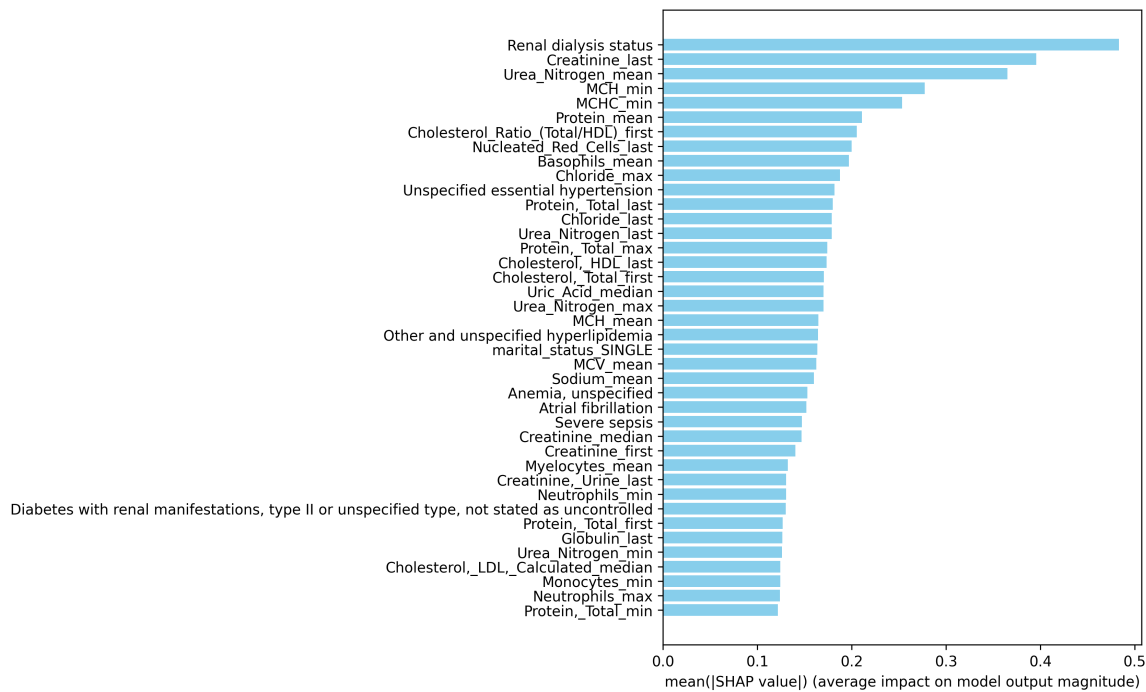


Figure 5: Top 40 mean absolute SHAP values from LR model.

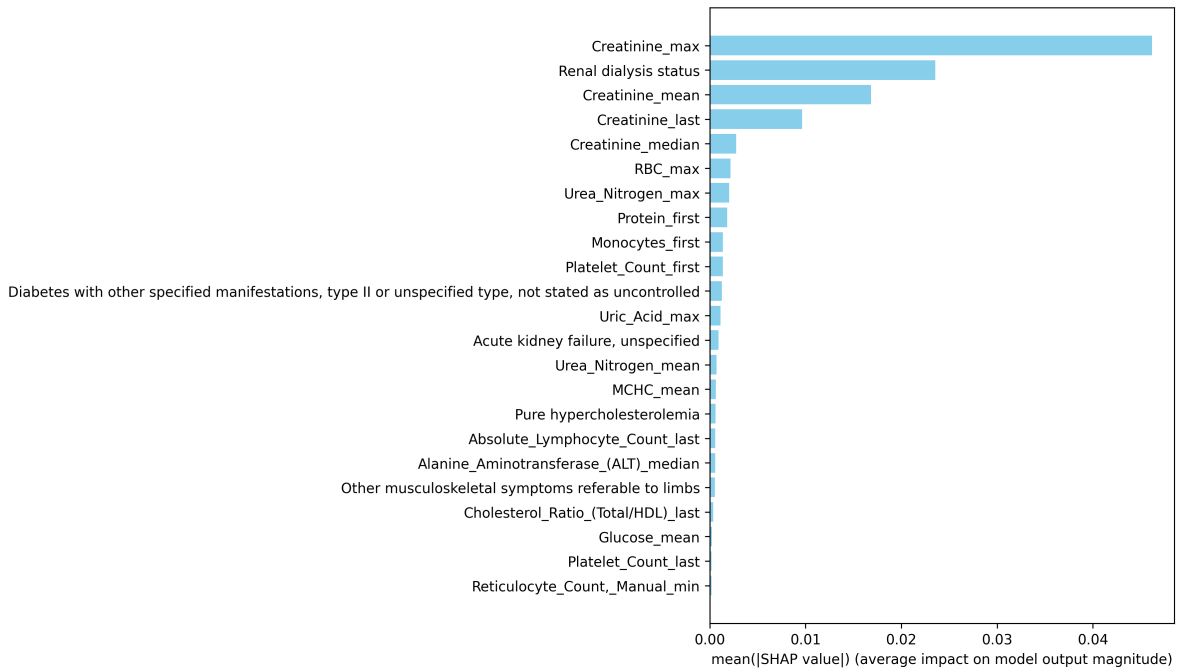


Figure 6: Top 40 mean absolute SHAP values from DT model.

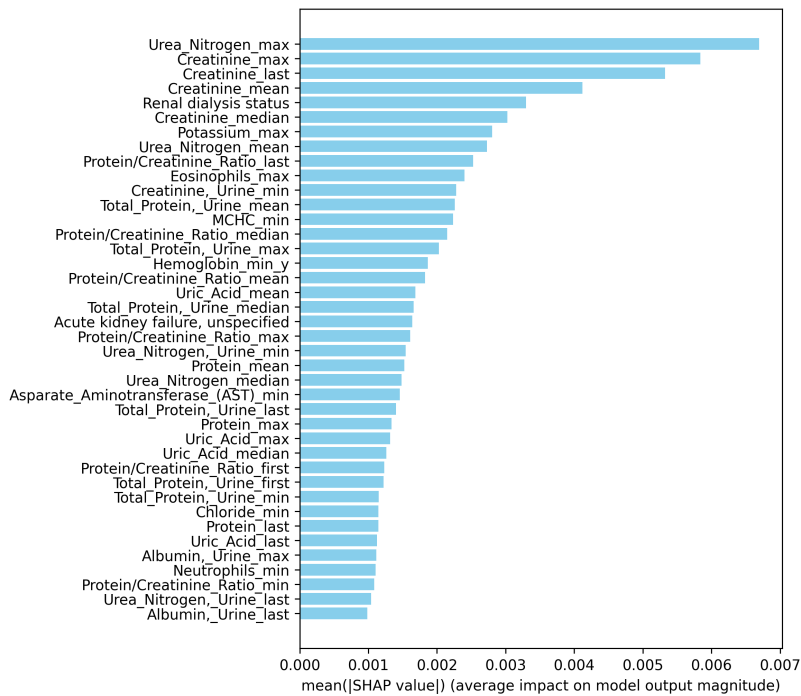


Figure 7: Top 40 mean absolute SHAP values from RF model.



## Appendix J. Brier Scores

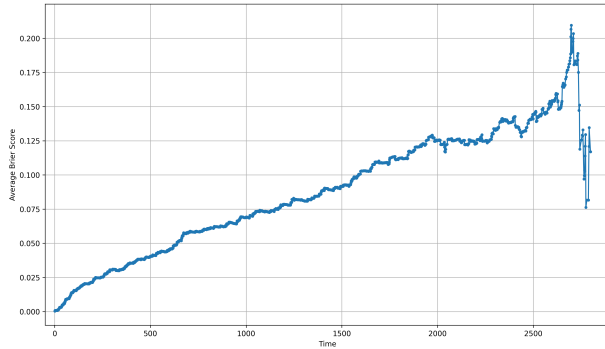


Figure 8: Brier score plot for baseline Cox model.

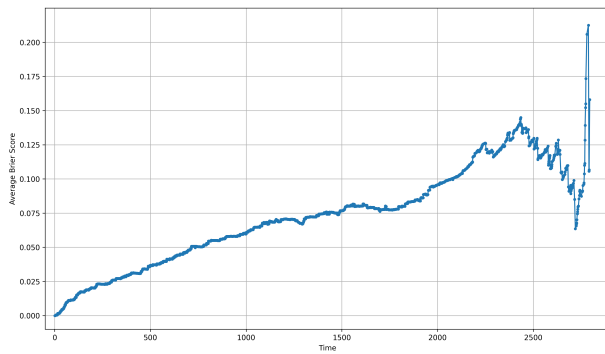


Figure 9: Brier score plot for XGboost-augmented Cox model.

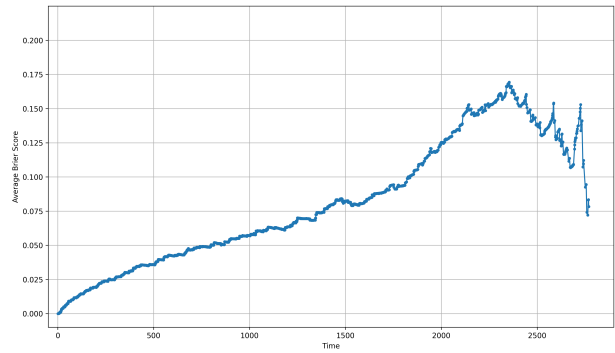


Figure 10: Brier score plot for FCNN-augmented Cox model.

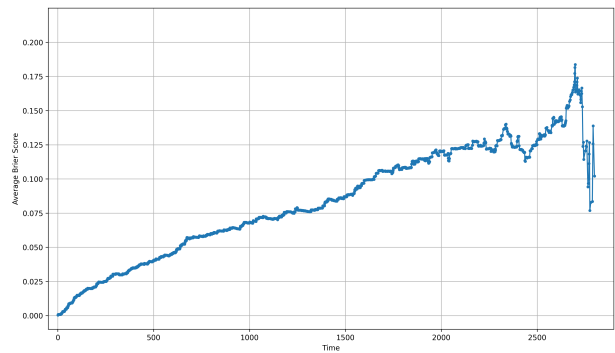


Figure 11: Brier score plot for ResNet-augmented Cox model.

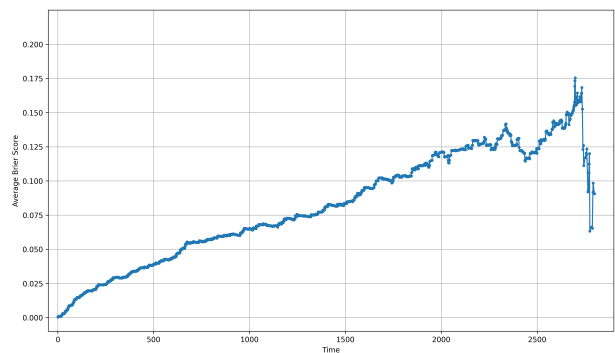


Figure 12: Brier score plot for LR-augmented Cox model.

### Appendix K. Dynamic AUC

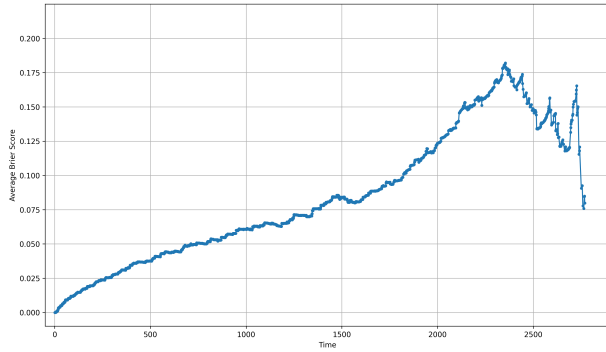


Figure 13: Brier score plot for FCNN-augmented Cox model.

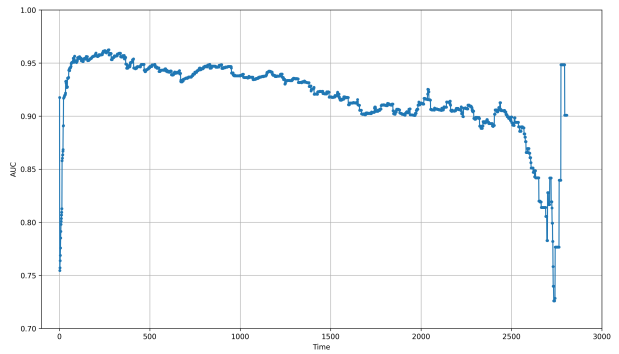


Figure 15: Time-dependent AUC plot for baseline Cox model.

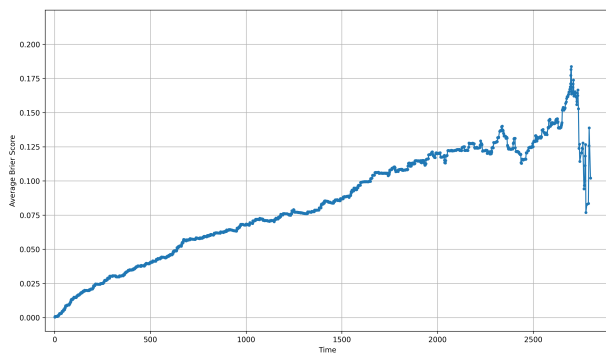


Figure 14: Brier score plot for ResNet-augmented Cox model.

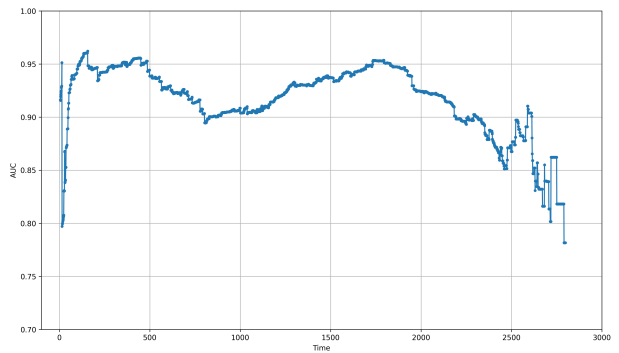


Figure 16: Time-dependent AUC plot for XGboost-augmented Cox model.

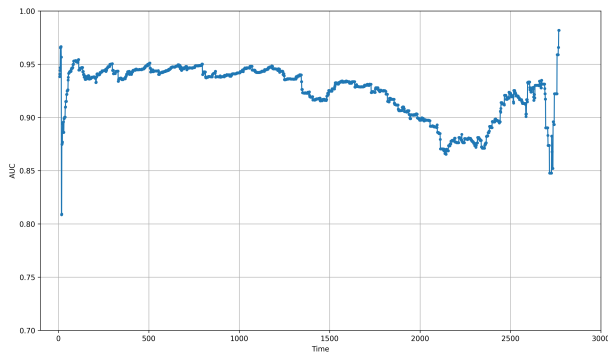


Figure 17: Time-dependent AUC plot for FCNN-augmented Cox model.

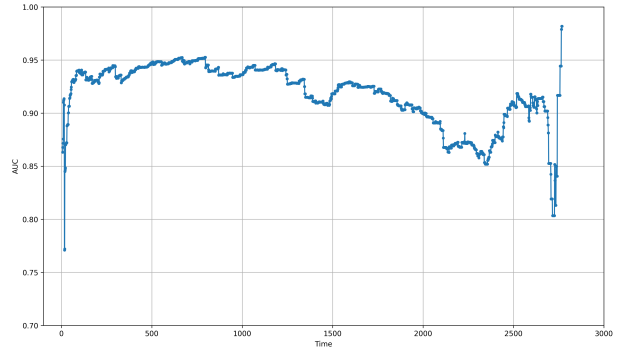


Figure 20: Time-dependent AUC plot for DT-augmented Cox model.

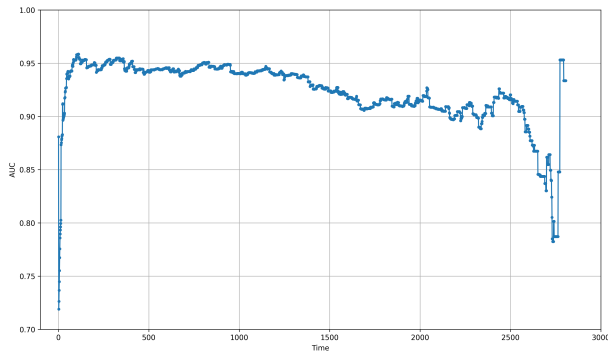


Figure 18: Time-dependent AUC plot for ResNet-augmented Cox model.

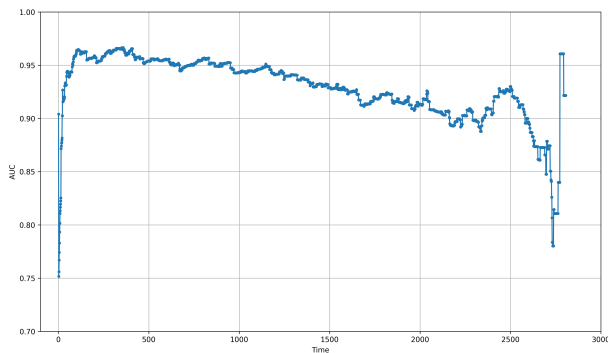


Figure 19: Time-dependent AUC plot for LR-augmented Cox model.

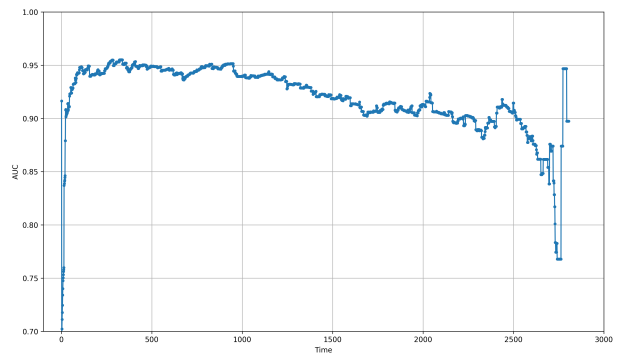


Figure 21: Time-dependent AUC plot for RF-augmented Cox model.